Available online at www.sciencedirect.com
SCIENCE DIRECT®
J. Vis. Commun. Image R. 15 (2004) 565–579
JOURNAL OF VISUAL Communication & IMAGE Representation
www.elsevier.com/locate/jvci

Combining a morphological interpolation approach with a surface reconstruction method for the 3-D representation of tomographic data

N. Mouravliansky, G.K. Matsopoulos,* K. Delibasis, P. Asvestas, and K.S. Nikita

Institute of Communication and Computer Systems, Department of Electrical and Computer Engineering, National Technical University of Athens, Athens, Greece

Received 5 March 2003; accepted 2 December 2003
Available online 22 January 2004

Abstract

In this paper, a new interpolation scheme, based on Mathematical Morphology and a modified Marching Cubes (MC) Algorithm to reconstruct 3-D anatomical structures is presented. The proposed interpolation technique is implemented using morphological operations and incorporates a distance function to improve the computational effectiveness of the technique. The morphological interpolation technique is compared to an existing shape based interpolation method and its advantages include superiority capability on handling various cases such as the branching and holes problem (appearance and disappearance of information) and more accurate volume estimation. Furthermore, the morphological technique is companied with a 3-D reconstruction algorithm capable of representing any anatomical structure from real 3-D medical data. Introducing a novel general rule, the algorithm triangulates all standard cube configurations introduced from the standard MC algorithm, without producing topologically incoherent surfaces or holes. Finally, the technique is implemented in JAVA and its output is in VRML 1.0 format; therefore it can be executed over the internet and implemented for telemedicine applications.

Keywords: Medical interpolation; Mathematical morphology; 3-D visualization; Surface reconstruction; Marching Cubes Algorithm

* Corresponding author. Fax: +30-210-772-2288.
E-mail addresses: nikos@isihellas.com (N. Mouravliansky), gmatso@esd.ece.ntua.gr (G.K. Matsopoulos).

1047-3203/$ - see front matter
doi:10.1016/j.jvcir.2003.12.003

1. Introduction

Medical image interpolation is a process often required for discrete image analysis, manipulation, and visualization. Various interpolation methods have been introduced for the image generation and more frequently for the image post-processing. In the latter, there are cases where interpolation techniques have been applied in order to reduce errors during monomodal or multimodal medical image registration (Meijering et al., 2001), to improve image quality due to an implementation of lossy image compression algorithm (Beucher, 1998), or to improve volumetric medical image representation from various medical imaging devices (Ostuni et al., 1997). In particular, three-dimensional (3-D) anatomical structures are commonly obtained from a sequence of cross-sectional slices (equally spaced 3-D samples) by contiguously scanning a 3-D region of the body. However, in clinical practice, it happens very often to collect a limited number of slices in order to reduce the patient's exposure and the examination time. Additionally, there are cases where the spacing between slices is not uniformly distributed, resulting in an anisotropic data set. Since most of the visualization techniques operate on equally spaced 3-D samples, a medical image interpolation technique becomes inevitable.

Broadly, interpolation techniques can be divided in two categories: gray level interpolation and binary interpolation methods. In gray level based methods, the interpolated values are determined directly from the gray values of neighboring image elements. Examples of methods belonging to this category are: nearest neighbor, linear, quadratic, cubic, spline family, Lagrange polynomials, truncated sinc, etc. (Meijering et al., 2001; Lehmann, 1999; Thevenaz et al., 2000). The gray level interpolation is based generally on the assumption that if a small change of the shape of object occurred then it would result a small change of the chromatic density of the object. This is sufficient when the images acquired from a modality are dense (e.g., MRI of the brain with resolution $1 \times 1 \times 3$ mm). Medical data are often quite sparse and the application of the gray level interpolation in these data creates blurred intermediate slices and/or it assigns to area intermediate colors that corresponds to artifacts.

Shape based interpolation techniques are object based and applied on structures of interest according to their geometrical characteristics, after a segmentation procedure is applied. In object based methods, some object information is extracted from the given data and is used in guiding the interpolation process. An example of method belonging to this category is that developed by Goshtasby et al. (1992), where correspondence between feature points is used in directing the interpolation process. An efficient binary interpolation algorithm was introduced in (Raya and Udupa, 1990). The algorithm consists of first segmenting (using thresholding) the given image data into a binary image and then converting the binary image back into a gray image wherein the gray value of a point represents its shortest distance from the cross-sectional boundary (positive for the points of object and negative for those outside) (Rausin, 1995). After acquiring the signed distance maps of the two sequential contours, a linear interpolation is performed generating a set of intermediate distance maps according to the required resolution. Then, the inverse procedure is performed

creating form the distance maps the binary contour interpolating slices. This algorithm, proposed in (Raya and Udupa, 1990), is also implemented for comparison purposes and it will be referred as shape based interpolation in the rest of the paper. Other interpolation methods on binary objects are based on elastic dynamic interpolation (Burr, 1981; Chen et al., 1990) and direction interpolation, called staircase (Werahera et al., 1995). These algorithms have difficulties when dealing with non-convex objects and the computational requirements are enormously increased.

Interpolation techniques have been also used on binary, mosaic, gray level, and color images, based on mathematical morphology (Serra, 1983, 1988. These methods were consisted by creating intermediary two-dimensional images between two given ones by morphological filtering. Morphological interpolation approaches were based on the application of either a morphological median (Meijering et al., 2001; Iwanowski and Serra, 1999), or using an interpolation function which describes the relative distance between the objects (Meyer, 1996). In terms of interpolating binary images, a major drawback of these methods is that the intersection of the input objects must be non-empty. The Hausdorff distance was also incorporated for interpolating images in (Serra, 1998), which allows interpolation between disjoint input objects but it creates large interpolated objects compared with the input ones. Furthermore, an interpolation method, trying to correct the disadvantage of the previous method, was introduced implementing in (Iwanowski, 2002). According to this method, a geodesic set is used covering both input objects as well as the gap between them. Then, interpolation sets are created by the implementation of morphological dilations of the geodesic set controlled by a distance function. The algorithm does not deal with interpolation of on non-convex objects where irregularities or holes and concavities are presented, as they often occurred in clinical medical data.

Another shape based interpolation technique was performed for two adjacent slices using mathematical morphology operations and conditional erosions applied iteratively (Joliot and Mazoyer, 1993). After segmentation, the two slices are scanned and three regions are identified containing common, non-common and intermediate points, respectively. Since the intermediate slice must contain the common points and part of intermediate points, iterative erosions of the intermediate points by 3×3 structuring element are applied until a required number of points is achieved. The algorithm fails if there is a cavity present in start slice, which disappears in the goal. To correct this drawback the algorithm requires the identification and skeletonization of these components and the removal of the skeleton points. Even with these corrections, the algorithm loses its attraction because the skeletonization is a complex morphological procedure and is often difficult to recognize areas that require the above transformation. Furthermore, this interpolation technique is applied in order to interpolate only MRI brain data and it was not extensively tested to other general cases that occur in medical imaging.

In this paper, a 3-D medical imaging representation scheme is presented. The scheme consists of the novel implementations of two algorithms for interpolating and reconstructing medical data from different imaging modalities. The first algorithm is an interpolation algorithm based on mathematical morphology capable of handling various cases occurring on medical data, including the branching and holes

problem as well as the accurate volume representations. The second algorithm, as a reconstruction algorithm, consists of a modification of the standard MC algorithm and it is capable to fast and efficient reconstruct 3-D medical structures. The medical representation scheme is successfully validated on several synthetic data as well as on real medical data providing 3-D medical data to further used for various telemedicine applications.

2. The proposed morphological interpolation algorithm

Creation of intermediate slices, between a start and a goal slice, resembles to existing multiresolution image representation and decomposition schemes where a sequence of images with decreasing resolution is treated. Morphological filters have been applied in each step of these schemes preserving edge and features properties in various applications (Haralick et al., 1987; Matsopoulos and Marshall, 1995). A modified version of these schemes is used based on the theory that binary operators are equivalent with thresholding the distance map of an image (Liang et al., 1989).

The first step of the algorithm is the segmentation process. The seeded region growing technique (Adams and Bischof, 1991) is firstly applied in the 3-D data. Given the seed, the algorithm finds a tasselation of the 3-D image into regions with the property that each connected component of a region meets exactly the initial seed point. Subject to this constraint, the region is chosen to be as homogeneous as possible. Binary contours of the object are then obtained.

Let call S_0 and S_{n+1} the start and the goal slices, O_0 and O_{n+1} the set of points that belong to the object from the corresponding slices and B_0 and B_{n+1} the set of points that belong to the background.

We first generate the signed (positive values for the inner area of the objects and negative values for the outer of the objects) city block distance map for each slice S_0 and S_{n+1}, noted as $DM(S_0)$ and $DM(S_{n+1})$, respectively. A fast calculation of the distance map is presented in Appendix A. Then, the difference of the two slices S_0 and S_{n+1} is obtained, (S_0/S_{n+1}). The points of the union of the two objects are labeled as follows:

P_c *if a point belongs to* $O_0 \cap O_{n+1}$ *set*,
P_- *if a point belongs to* O_{n+1}/O_0 *set*,
P_+ *if a point belongs to* O_0/O_{n+1} *set*,

where $\cap$ denotes set intersection and / set difference.

The information from S_0 to S_{n+1} then is used in order to calculate the distance map histograms for the inner points of the objects labeled as P_- and P_+, respectively. Analytically, H_1 is the histogram that contains the density values of the $DM(S_0)$ having a range of positive values from 1 to $h_{1\max}$ and H_2 is the histogram that contains the density values of the $DM(S_{n+1})$, having a range of positive values from 1 to $h_{2\max}$.

Then, the number of points that must be contained in the interpolating slices is calculated. Let N_C the number of points labeled as P_C, N_+ the number of points labeled as P_+, and N_- the number of points labeled as P_-. The total number of points, N_{TOTAL}, for the intermediate slice for level i, with $i = 1, \ldots, n$, is given:

$$N_{\mathrm{TOTAL}} = N_{\mathrm{C}} + N_{-}\frac{i}{n+1} + N_{+}\frac{(n+1)-i}{n+1}, \tag{1}$$

where N_{C} is the number of points labeled P_{C}, N_{-} is the number of points labeled P_{-}, N_{+} is the number of points labeled P_{+}.

The number of points, N, which are inner points of both objects and they are candidates to be morphologically transformed, are given from the following equation:

$$N = N_{-} + N_{+}. \tag{2}$$

In order to generate the intermediate slices, we take as a reference slice the start, S_0, slice. Each intermediate slice must contain the common points, P_{C}, of the slices S_0 and S_{n+1} and a number of points labeled as P_{-} and P_{+} from the S_0/S_{n+1}. In each intermediate slice i, the P_{-} points must be generated and the P_{+} points must be reduced. This resembles to the morphological operations of erosion and dilation under certain constrains.

A threshold t_1 is defined from the histogram H_1 in such a way that pixels between *1* and t_1 have a number of $N_{-}(i) = N_{-}(i/(n+1))$ and a threshold t_2 for the histogram H_2 is defined is such a way that pixels between the threshold t_2 and $h_{2\max}$ have a number of $N_{+}(i) = N_{+}(((n+1)-i)/(n+1))$ points.

In order to produce an interpolation slice at level i, morphological erosion and dilation operations are implemented under certain constrains. Specifically, the reduction of P_{+} points corresponds to the morphological erosion of these points by B_{t_1}, where B_{t_1} is an elementary structuring element with diamond shape and size t_1, equals to the threshold level of histogram H_1. This operation is equivalent with thresholding the distance map of S_0 with threshold t_1 by keeping all points of the distance map with value larger than t_1 as object points:

$$P_{+} \ominus B_k \approx \ \mathrm{thresh}(DM(S_0), t_1), \tag{3}$$

where $\mathrm{thresh}(DM(S_0), t_1) = 1$, if $DM(S_0) > t_1$, and 0 otherwise.

Similar, the generation of P_{-} points corresponds to the dilation of these points with, B_{t_2}, where B_{t_2} is an elementary structuring element with diamond shape and size t_2, equals to the threshold level of histogram H_2. This operation is equivalent with thresholding the distance map of S_{n+1} with threshold t_2 by keeping all points of the distance map with value lower than t_2 as object points:

$$P_{-} \oplus B_k \approx \ \mathrm{thresh}(DM(S_{n+1}), t_2), \tag{4}$$

where $\mathrm{thresh}(DM(S_{n+1}), t_2) = 1$, if $DM(S_{n+1}) < t_2$, and 0 otherwise.

Then, the final interpolating slice of level i is produced adding in the initial slice S_0, the P_{-} points with distance map value lower than t_1 (dilation under constrains) and subtracting from the initial slice S_0 the P_{+} points with value larger that t_2 (erosion under constrains).

The new interpolation scheme is presented in Fig. 1. The proposed algorithm was tested on generated images, producing the results shown in Fig. 2, covering various cases such as changing of size, translation, disappearance of information, and appearance and disappearance of holes from one slice to the next one.

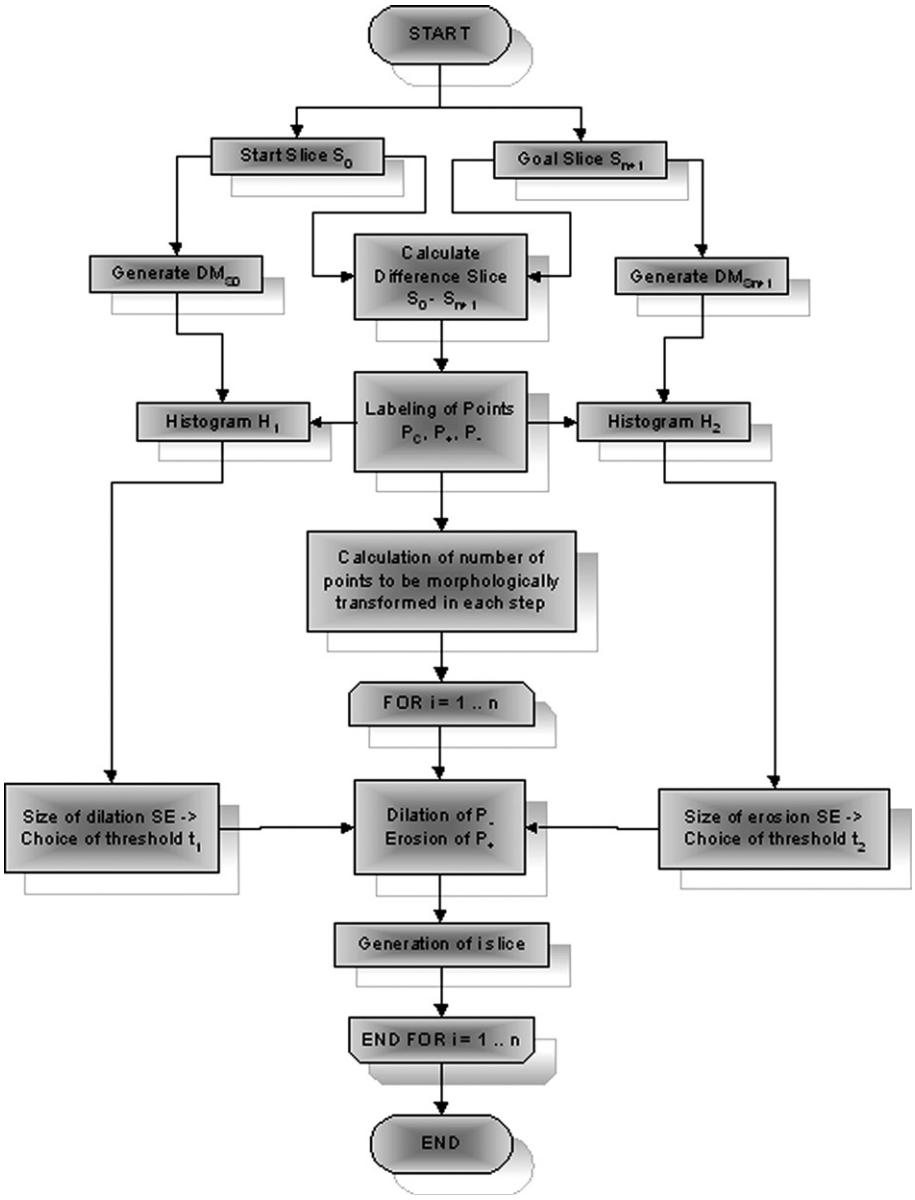

Fig. 1. Flow chart of the new Morphological interpolation algorithm.

3. A modified marching cubes algorithm for surface rendering

Surface reconstruction consists the final step of the proposed 3-D image representation scheme. To this end, a surface rendering technique, based on the modification of the MC algorithm, is used, producing VRML format files

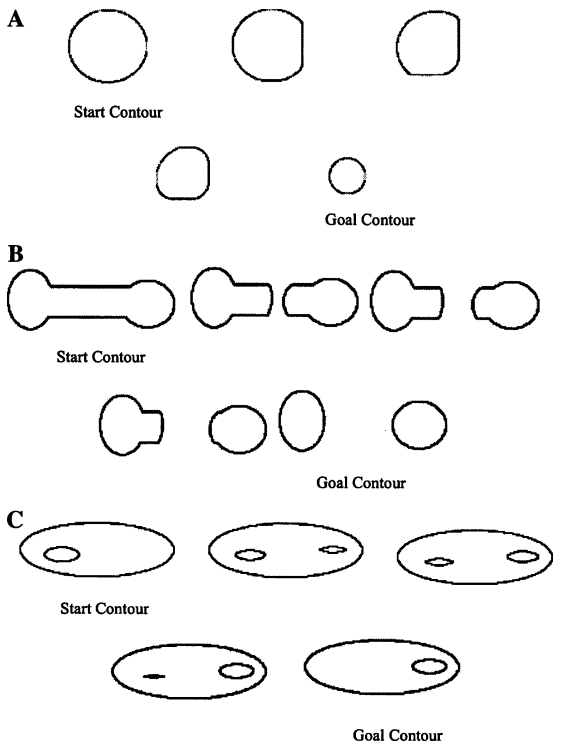

Fig. 2. (A–C) Application of the proposed morphological interpolation algorithm (creation of three intermediate slices) in three test patterns. The first pair of contours (A) covers the case of a simple changing of the size and translation of an object. The second pair (B) is the case of the appearance or disappearance of part of an object. The third pair (C) is the case of objects with the appearance and the disappearance of holes.

suitable for telemedicine applications. Next, the modified MC algorithm is shortly described.

Given a gray scale 3-D image, the standard MC algorithm produces an isosurface of value t (Lorensen and Cline, 1987). The algorithm operates on a standard length (usually voxel) cubic region of the image that occupies 8 adjacent voxels. The vertices of the cube are set to *1*, if the value of the corresponding image voxel is greater than or equal to the threshold t, and *0* otherwise. The pattern produced is called "Cube Configuration." There are a number of 256 possible configurations, which have been reduced to 14, using symmetry (Baker, 1989). The symmetry is defined as the equivalence between complementary configurations (if the action of the logical not operator on the one of them generates the other).

The standard MC algorithm can be summarized in pseudocode as follows:

FOR each image voxel

a cube of length 1 is placed on 8 adjacent voxels of the image

FOR each of the cube's edge{

IF (the one of the node voxels has value greater than or equal to t
AND the other voxel has value less than t) THEN
{calculate the position of a point on the cube's edge that
belongs to the isosurface, using linear interpolation}
}
FOR each of the predefined cube configurations{
FOR each of the 8 possible rotations{
FOR the configuration's complement{
{compare the produced cube configuration of the above
calculated iso-points to the set of predefined cube
configurations and produce the corresponding triangles}
}
}
}

In the case of a binary image with threshold t, the iso-points lie necessarily on the middle of the cube's edges, for which the two voxels had the values of *0* and *1*. When the input is a gray scale image and the two cube vertices (image voxels) have values n_1 and n_2 satisfying the inequality: $(t - n_1)(t - n_2) \leqslant 0$, the location of the iso-point is calculated using linear interpolation along the edge connecting the two voxels. The main drawback of this implementation is the computational overhead imposed by the cube relations and comparisons as well as the great number of the produced triangles. From a programming point of view, this method of predefining cube configuration and their connected triangles is error prone. Furthermore, the use of symmetry produces topologically incoherent surfaces, or holes in certain cases of two adjacent cubes (Zhou et al., 1994).

In this paper, a novel implementation is used, based on a single rule capable of generating all predefined cube configurations. The modified algorithm uses the same first step, as the standard MC algorithm, with the addition that for each iso-point that is found, the voxel from which it stems is also kept. The voxel is called source voxel.

The implementation of the modified algorithm can be described in pseudocode as follows:

Step 0 *FOR each image voxel*
A cube of length 1 is placed on 8 adjacent voxels of the image
FOR each of the cube's edge
IF (the grey value of one of the edge node voxels is above t and
the other below t) THEN
Step 1 *{calculate the position of the iso-point on the cube's edge using*
linear interpolation;
place the iso-point into a list}
p = 0
Step 2 *Scan the list of iso-points until the first unmarked iso-point is found*
IF no unmarked iso-points exist in the list THEN GO TO **Step 0**
ELSE
p = p+1

set the first unmarked iso-point as current_iso-point
mark current_iso-point as belonging to polygon p
new_iso-point = next_iso-point(current_iso-point)
WHILE (new_iso-point<>NULL)
new_iso-point = next_iso-point(current_iso-point)
current_iso-point = new_iso-point
mark current_iso-point as belonging to polygon p
END
store the polygon into the VRML file
GO TO **Step 2**
END FOR (*each image voxel*)

It can be proved that the modified algorithm generates all the cases that are predefined by the standard MC algorithm. The only difference is that the produced output consists of polygons instead of triangles, but with their points equivalently ordered. Furthermore, the algorithm can handle cases where more than one polygon is present in the same cube. As the modified algorithm does not depend on the complementary symmetries, it does not suffer from specific type of holes, "type A," that appear due to the symmetry. A full verification of the modified MC algorithm and comparison with other surface rendering techniques is presented in (Delibasis et al., 2001).

4. Experimental results

The proposed morphological interpolation algorithm was tested on isotropic axial CT and MRI data sets with pixel size $1 \times 1 \times 1$ mm (slice spacing uniform) and scan dimensions $256 \times 256 \times 98$ and $256 \times 256 \times 85$, respectively. The seeded region growing algorithm was firstly applied on the 3-D data in order to isolate the skull region from the CT data and the brain area from the MRI data. The data sets were subsampled subtracting one up to six intermediate slices. Then, the shape based (Raya and Udupa, 1990) and the proposed morphological interpolation algorithms are performed. Quantitative measurements are introduced counting the percentage of the absolute errors, in term of number of volume and surface points, of the reconstructed data sets from the initial ones, according to the following equation:

$$E_V = \left| \frac{V_0 - V_i}{V_i} \right| x\ 100\% \text{ and } E_S = \left| \frac{S_0 - S_i}{S_i} \right| x\ 100\%, \tag{5}$$

where V_0 and V_i are the original and the reconstructed volumes, S_0 and S_i are the original and the reconstructed surfaces and E_V and E_S the absolute errors of volumes and surfaces. The results are presented in Table 1 and Table 2 whereas in Fig. 3 shows the percentage of absolute errors for the two interpolation methods. In Tables 1 and 2, the percentage of the absolute errors by applying the two interpolation methods are presented, in term of volume and surface. The results are obtained interpolating one up to six slices in the original CT and MRI data, respectively. Also, in Fig. 3, it can be seen that the loss of points follows the number of interpolating

Table 1
Percentage of the absolute error applying the shape based and the proposed morphological interpolation algorithms on original CT data

SKULL							
Number of interpolating slices		1	2	3	4	5	6
E_V (%)	Shape based Interpolation	11	22	22	26	29	31
	Morphological Interpolation	2	1	2	2	1	1
E_S (%)	Shape based Interpolation	10	15	20	25	30	32
	Morphological Interpolation	2	5	8	11	12	13

Table 2
Percentage of the absolute error applying the shape based and the proposed morphological interpolation algorithms on original MRI data

BRAIN							
Number of interpolating slices		1	2	3	4	5	6
E_V (%)	Shape based Interpolation	9	13	14	16	17	17
	Morphological Interpolation	2	2	3	3	3	4
E_S (%)	Shape based Interpolation	15	21	25	28	32	32
	Morphological Interpolation	7	11	16	18	22	22

slices. Analytically, for the shape based interpolation method (linear interpolation), the absolute volume and surface errors follow the subsampling rate resulting a loss of the volume points compared to the original. In contrast, the morphological interpolation method tends to preserve the volume of the objects uncorrelated with the subsampling rate as it controls the number of points from the calculated from the distance histograms. In terms of surface error, the morphological interpolation method follow the subsampling rate but it behaves better than the shape based interpolation method. These can become clear looking at real 3-D rendered data using the modified MC algorithm (Fig. 4 and Fig. 5), where the loss of points follows the number of interpolating slices.

5. Conclusions

In this paper, we have presented a new scheme for representing 3-D tomographic data from various medical imaging modalities. The scheme is based on the application of a new interpolation algorithm based on Mathematical Morphology and a modified MC algorithm for the 3-D rendering of the data.

The proposed morphological interpolation algorithm provides more accurate quantitative measures resulting enhanced representations than the shape based interpolation. It also covers all the possible cases that can be found from the start to a goal slice, including the branching and the holes problem. Because is using morpho-

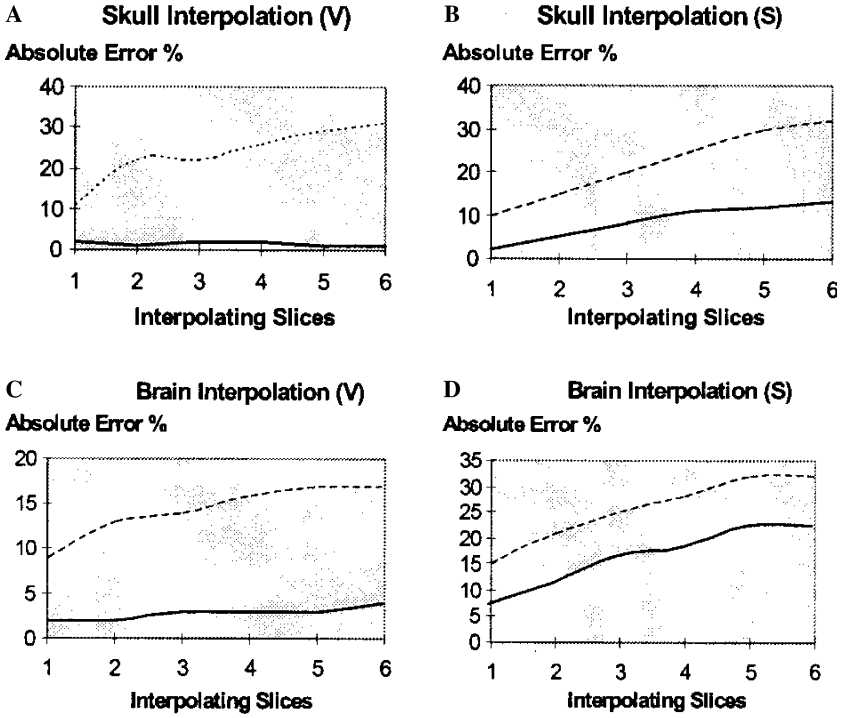

Fig. 3. Volume absolute error using the proposed morphological interpolation technique (continuous line) and the shape based interpolation technique (dotted line). (A–C) Interpolation of skull and brain. Surface absolute error using the proposed morphological interpolation technique (continuous line) and the shape based interpolation technique (dotted line). (B–D) Interpolation of skull and brain.

logical operations, it is simple and can be incorporated easily with imaging modalities used in clinical practice.

Furthermore, the modified MC algorithm is independent from any predefined cube configurations. The proposed surface rendering uses a generic rule capable of generating the correct polygons in any case of configurations without introducing "type A" hole problems, which occur in the standard MC algorithm. Finally, the algorithm is implemented on Java, generating output files in VRML format from 3-D medical data sets. It is therefore suitable for platform independent applications, such as the Telemedicine applications.

Appendix A. Fast calculation of city block distance map

The algorithm is initialized putting all the contour points in a list and assigning value 1 to the points of the contour and value 0 elsewhere. Then, an iteration begins extracting in each step the first point of the list. All its neighbors (following the four neighbors connectivity), which are not assigned with a value take a value, equal to

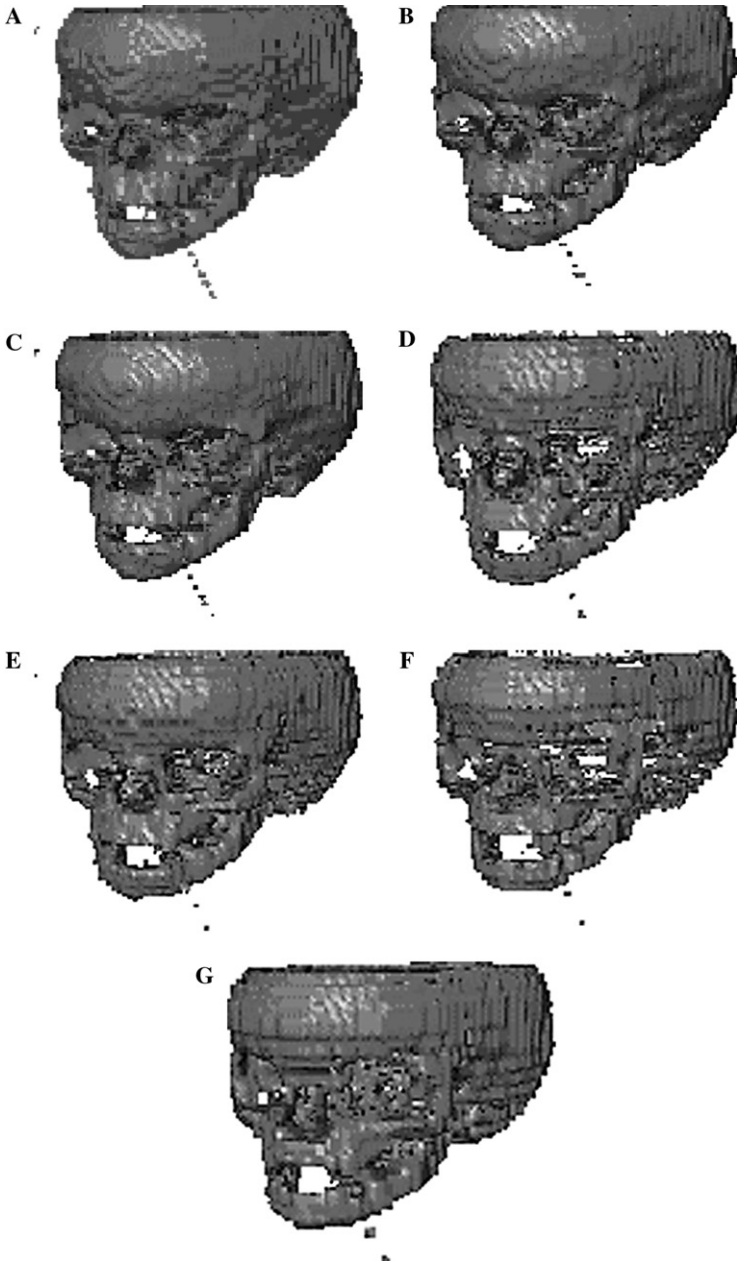

Fig. 4. (A–F) Surface rendering of subsampled CT skull data set using the modified MC algorithm (VRML output files). (A) 3-D model produced by the full resolution data. (B, D, and F) 3-D models produced using the shape based interpolation algorithm and subsampling on, three, and five slices, respectively. (C, E, and G) 3-D models produced using the morphological interpolation algorithm and subsampling one, three or five slices, respectively.

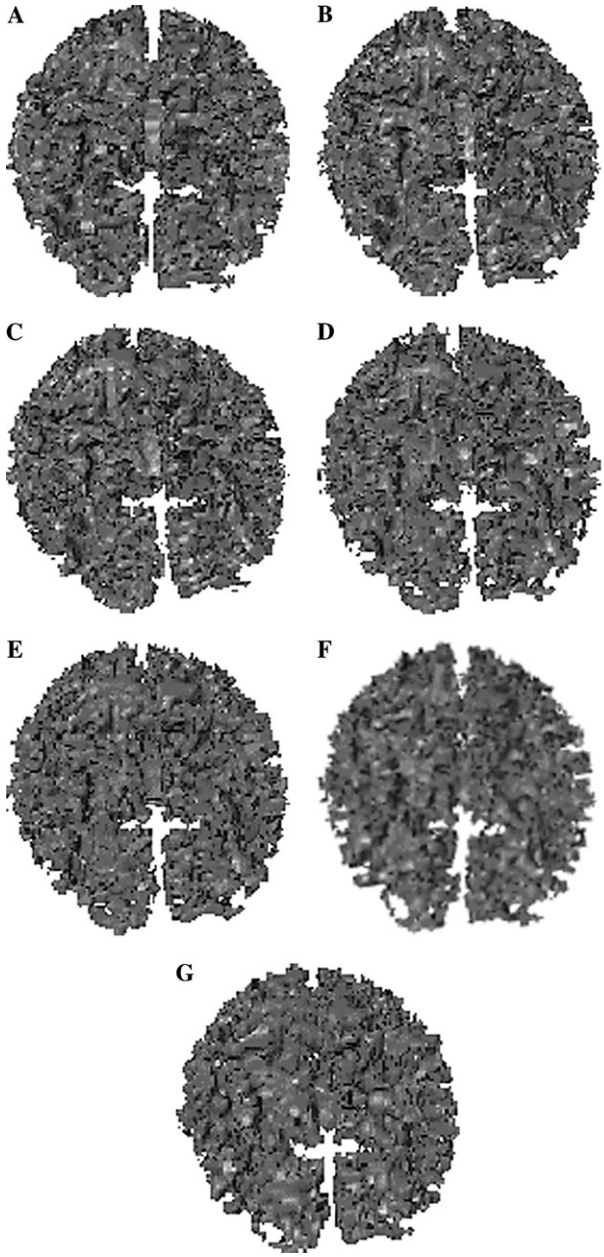

Fig. 5. (A–f) Surface rendering of subsampled MRI brain data set using the modified MC algorithm (VRML output files). (A) 3-D model produced by the full resolution data. (B, D, and F) 3-D models produced using the shape based interpolation algorithm and subsampling on, three, and five slices, respectively. (C, E, and G) 3-D models produced using the morphological interpolation algorithm and subsampling one, three or five slices, respectively.

the value of the extracted point plus one and they are put in the list. The iteration stops when all points of the map have a value. The implementation of the algorithm is described as follows:

```
initialize the linear list
put all contour points in the linear list
give to their position on the map value 1
while list not empty
{
   put out the first point of the list
   dist = value of the distance map of the pixel
      for each neighboring pixel
           {
           if the distance map is not assigned with a value{
           assign the distance map with value = dist + 1
           put the pixel in the list}
           }
}
multiply points not belonging to the object on the distance map with -1.
```

References

Adams, R., Bischof, L., 1991. Seeded region growing. IEEE Trans. Pattern Anal. Mach. Intell. 16, 641–647.

Baker, H.H., 1989. Building surfaces of evolution: the weaving wall. Int. J. Comp. Vis. 3, 51–71.

Beucher, S., 1998. Interpolation of sets, of partitions and of functions. In: Heijmans, H., Roerdink, J. (Eds.), Mathematical morphology and its application to image and signal processing. Kluwer, Dordrecht.

Burr, D.J., 1981. Elastic matching of line drawings. IEEE Trans. Pattern Anal. Mach. Intell. 3, 708–713.

Chen, S.Y., Lin, W.C., Liang, C.C., Chen, C.T., 1990. Improvement on dynamic elastic interpolation technique for reconstructing 3-D objects from serial cross sections. IEEE Trans. Med. Imag. 9, 71–83.

Delibasis, K.S., Matsopoulos, G.K., Mouravliansky, N., Nikita, K.S., 2001. A novel and efficient implementation of the marching cubes algorithm. Comp. Med. Imaging Graph. 25, 343–352.

Goshtasby, A., Turner, D.A., Ackerman, L.V., 1992. Matching of tomographic slices for interpolation. IEEE Trans. Med. Imag. 11, 507–516.

Haralick, R.M., Lin, C., Lee, I.S.S., Tcang, X., 1987. Multiresolution Morphology. In: Proceedings 1st International Conference in Computer Vision. London, England, pp. 516–520.

Iwanowski, M., Serra, J., 1999. Morphological interpolation and color images. In: Proceedings of 10th International Conference on Image Analysis and Processing ICIAP'99. Venice, Italy, pp. 50–55.

Iwanowski, M., 2002. Morphological binary interpolation with convex mask. In: Proceedings of International Conference on Computer Vision and Graphics. Zakopane, Poland, pp. 360–367.

Joliot, M., Mazoyer, B.M., 1993. Three-dimensional segmentation and interpolation of magnetic resonance brain images. IEEE Trans. Med. Imag. 12, 269–277.

Lehmann, T.M., Gönner, C., Spitzer, K., 1999. Survey: interpolation methods in medical image processing. IEEE Trans. Med. Imag. 8, 1049–1075.

Liang, J.I., Piper, J., Tang, J.Y., 1989. Erosion and dilation of binary images by arbitrary structuring elements using interval coding. Pat. Recog. Let. 9, 201–209.

Lorensen, W.E., Cline, H.E., 1987. Marching cubes: high resolution 3D surface construction algorithm. Comp. Graph. 21, 163–169.

Matsopoulos, G.K., Marshall, S., 1995. Application of morphological pyramids: fusion of MR and CT phantoms. J. Visual Com. Image Rep. 6, 196–207.

Meijering, E.H.W., Niessen, W.J., Viergever, M.A., 2001. Quantitative evaluation of convolution-based methods for medical image interpolation. Med. Image Anal. 5, 111–126.

Meyer, F., 1996. Morphological interpolation method for mosaic images. In: Maragos, P., Schafer, R.W., Butt, M.A. (Eds.), Mathematical morphology and its application to image and signal processing. Kluwer, Dordrecht.

Ostuni, J.L., Santha, A.K.S., Mattay, V.S., Weinberger, D.R., Levin, R.L., Frank, J.A., 1997. Analysis of interpolation effects in the reslicing of functional MR images. J. Comput. Assist. Tomogr. 21, 803–810.

Rausin, P.L., 1995. Salience distance transform. Graph. Models Image Process. 57, 483–521.

Raya, S.P., Udupa, J.K., 1990. Shape based interpolation of multidimensional objects. IEEE Trans. Pattern Anal. Mach. Intell. 9, 32–42.

Serra, J., 1983. Image Analysis and Mathematical Morphology, vol. 1. Academic Press.

Serra, J., 1988. Image Analysis and Mathematical Morphology, vol. 2. Academic Press.

Serra, J., 1998. Hausdorff distance and interpolations. In: Heijmans, H., Roerdink, J. (Eds.), Mathematical morphology and its application to image and signal processing. Kluwer, Dordrecht.

Thevenaz, P., Blu, T., Unser, M., 2000. Interpolation revisited. IEEE Trans. Med. Imag. 19, 739–758.

Werahera, P.N., Miller, G.J., Taylor, G.D., Brubaker, T., Danesghari, F., Crawford, E.D., 1995. A 3-D reconstruction algorithm for interpolation and extrapolation of planar cross sectional data. IEEE Trans. Med. Imag. 14, 765–771.

Zhou, C., Shu, R., Kankanhalli, M.S., 1994. Handling small features in isosurface generation using marching cubes. Comp. Graph. 18, 845–848.